Final Report for:

CONTRACT N00014-97-1-0966

SIGNAL SUBSPACE PROCESSING OF UNCALIBRATED MTD-SARS

Submitted to:

William J. Miceli
ONR IFO
PSC 802 Box 39
FPO AE 09499-0700
London, U.K.

Office of Naval Research
G. D. McNeal
Ballston Centre Tower One
800 North Quincy Street
Arlington, VA 22217-5660

Administrative Grants Officer
Office of Naval Research Regional Office Boston
495 Summer Street, Room ~~103~~ 627
Boston, MA 02210-2109

Director, Naval Research Laboratory
Attn: Code 2627
4555 Overlook Drive
Washingon, DC 20375-5326

Defense Technical Information Center
8725 John J. Kingman Road, STE 0944
Ft. Belvoir, VA 22060-6218

Distribution Statement:

Approved for public release.

Project Director:

Mehrdad Soumekh
Department of Electrical Engineering, 332 Bonner Hall
State University of New York at Buffalo
Amherst, New York 14260
Phone: (716) 645-2422, extension 2138
Fax: (716) 645-3656
Email: msoum@eng.buffalo.edu

1a. Summary

This document describes the final report for the work performed for "Signal Subspace Processing of Uncalibrated MTD-SARs," under Contract N00014-97-1-0966 for the Office of Naval Research.

This report provides a study on the merits of the algorithms that we have developed under this contract. For this purpose, we present moving target detection and imaging results for an X band spotlight SAR system that utilizes an along-track monopulse configuration for its data collection. The theoretical foundation of the processing that is used on these data is based on our work for this contract in which a two-dimensional signal subspace processing (adaptive filtering) method was developed to calibrate the monostatic and bistatic radars of the monopulse SAR system. The blind calibration of the two channels enables the user to null the stationary scene, and detect the moving targets. Next, a measure that we call SAR ambiguity function is used to estimate the relative speed of a detected moving target. The resultant estimate is then used to image the moving target.

1b. Publications

The work has produced the following publications:

M. Soumekh, "Moving Target Detection and Imaging Using an X Band Along-Track Monopulse SAR," scheduled to appear in *IEEE Transactions on Aerospace and Electronic Systems*, vol. 38, no. 1, January 2002.

M. Soumekh and B. Himed, "SAR-MTI Processing of Mutli-Channel Airbrone Radar Measurement (MCARM) Data," to appear in *Proceedings of IEEE International Conference on Radar Systems,"* Long Beach, May 2002.

M. Soumekh, "Wavefront-Based Synthetic Aperture Radar Signal Processing," *Frequenz*, pp. 99-113, March/April 2001 (invited paper for the special issue on *Synthetic Aperture Radar*).

M. Soumekh, "UHF-Band P-3 and X-Band Monopulse-GMTI SAR Processing," *Proceedings of European Conference on Synthetic Aperture Radar*, pp. 185-188, Munich, May 2000.

G. Genello, M. Wicks and M. Soumekh, "Some interesting aspects of adaptive airborne phased array radar: Achieving MTD using SAR," *Proceedings of Fifth International Conference on Radar Systems,"* Brest, France, May 1999.

M. Soumekh, "Signal Subspace Fusion of Uncalibrated Sensors with Application in SAR and Diagnostic Medicine," *IEEE Transactions on Image Processing*, vol. 8, no. 1, pp. 127-137, January 1999.

M. Soumekh, *Synthetic Aperture Radar Signal Processing,* New York: Wiley, 1999 (in print).

2. Introduction

Synthetic Aperture Radar (SAR) has become an important tool in military intelligence, surveillance and reconnaissance. With the advancement of sophisticated SAR signal processing and imaging methods, more specialized radar problems are being studied in the framework of SAR systems. A prominent example is ground moving target detection and imaging in a SAR scene. Earlier works by Raney [ran] and Kirk [kir] have provided fundamental signal theory tools to approach this problem; some of the recent works in this area are reported in [che], [mar], [per], [rao], [s95], and [yan].

One faces difficult practical problems in SAR detection and imaging of moving targets in the presence of stationary targets. A major impasse is that the image of a moving target in a reconstructed SAR image is smeared and weak in comparison to the SAR image of the surrounding stationary targets. Moreover, stationary targets commonly possess strong coherent signatures that overlap with the signature of the moving targets in the frequency domain; thus, the stationary targets signature cannot be filtered out.

A similar problem has been encountered in the conventional radar systems. A powerful and practical solution for this problem is the use of monopulse radar systems [can], [leo], [she]. An experimental phase-sum-and-difference monopulse radar was developed as early as 1958 in the United States to detect moving targets in vegetative clutter [leo, pp. 340-342]. Some of the extensions of this system are discussed in [she, Chapter 5]. It turns out that an along-track monopulse airborne radar (SAR) could also provide useful GMTI (ground moving target indicator) information [s97]; this is briefly described in Section 3. The main results of this report is on processing the along-track monopulse SAR data of an X band spotlight SAR system.

The user of a monopulse radar or SAR system runs into another practical problem that is related to the calibration of the two channels of the monopulse system; this is particularly difficult over a relatively long target interrogation (i.e., slow-time) in the SAR systems. This problem can be approached via relating the two monopulse channels via an *unknown*

calibration error function. The task is to blindly compensate for this miscalibration. This is a well-known problem in adaptive filtering [wid]. A practical and fast solution for the two-dimensional adaptive calibration of the two channels of a monopulse SAR system is suggested in [s99a]; this is reviewed in Section 4. Results on using this method on the along-track monopulse SAR data of the X band spotlight SAR system are then provided.

The task of imaging a detected moving target requires estimating a parameter related to the relative speed of the moving target with respect to the airborne radar. For this, we use a statistic that we refer to as SAR ambiguity function [s95]; this is shown in Section 5. Similar to the conventional ambiguity function, the SAR ambiguity function provides a measure that obtains its peak with the correct estimate of the the moving target speed value. Once the speed of a moving target is estimated, the user can use a high-resolution SAR imaging method to reconstruct the moving target [s99b]. The merits of these methods are studied using the along-track monopulse SAR data of the X band spotlight SAR system.

3. Along-Track Monopulse SAR

The along track monopulse SAR imaging system utilizes two radars for its data collection. One radar is used as a transmitter as well as a monostatic receiver. The other radar is used only as a bistatic receiver. In [s97], we documented a signal processing algorithm of the two monostatic and bistatic databases of the along track monopulse SAR system to obtain two *coherently* identical SAR images of the stationary targets in the scene. While the stationary targets appear the same in the monostatic and bistatic SAR images, however, the same is not true for moving targets.

This fact is the basis for developing a static, which we refer to as the difference image, for Moving Target Detection (MTD). If we denote the monostatic SAR image by $f_m(x,y)$ and the bistatic image by $f_b(x,y)$, the difference image for moving target detection is defined via the following:

$$f_d(x,y) = f_b(x,y) - f_m(x,y).$$

Numerical examples for an along track monopulse MTD-SAR system are shown in [s97].

These examples correspond to a realistic FOPEN SAR database which is injected with the simulated signatures of moving targets. For this simulation, the two radars are assumed to be fully calibrated; i.e., there is no relative gain and phase ambiguity in the data collected by the two radars. This idealistic scenario, however, is never encountered in

practice. In a realistic monopulse SAR system, the two radars exhibit different amplitude patterns (phase as well as gain) which vary with the radar frequency and the radar position (i.e., the slow-time). Moreover, these amplitude patterns vary from one pulse transmission to another due to heat and other uncontrollable natural factors which affect the internal circuitry of the two radars. These subtle changes of the radars amplitude pattern are difficult to be detected and tracked, and are unknown to the user.

As documented in [s99a], [s99b], we have developed a theoretical model for the undesirable variations of the amplitude pattern of uncalibrated monopulse radars and their effect in the difference image for MTD. This model indicates that the two monopulse SAR images of a *stationary* target (e.g., clutter and stationary vehicles) are related via

$$f_b(x,y) = f_m(x,y) \ ** \ h(x,y), \tag{1}$$

where $**$ denotes two-dimensional convolution in the spatial domain, and $h(x,y)$ is an *unknown* (miscalibration) impulse response which depends on the two radars calibration errors [99a]. Hence, one has to perform a *blind* calibration of the two images. A method for this using a two-dimensional adaptive filtering and its implementation via a signal subspace processing method are described in [s99a], [s99b, Chapter 8]; this is briefly outlined next.

4. Signal Subspace Processing for Moving Target Detection

A. Discrete Model

Adaptive filtering methods have been suggested to solve the above-mentioned blind calibration problem in one-dimensional cases [wid]. To apply these adaptive filtering methods in the two-dimensional problems, consider the discrete formed SAR image in the (x_i, y_j) domain. The impulse response $h(x,y)$ is modeled by a finite two-dimensional discrete filter h_{mn}; the size of the filter, call it (N_x, N_y), is chosen by the user based on a priori information. In the following discussion, we choose both N_x and N_y to be odd integers, and $(n_x, n_y) = (N_x/2 - .5, N_y/2 - .5)$. Then, the model in (1) is rewritten in the following discrete form

$$f_b(x_i, y_j) = \sum_{m=-n_x}^{n_x} \sum_{n=-n_y}^{n_y} h_{mn} \ f_m(x_i - m\Delta_x, y_j - n\Delta_y), \tag{2}$$

where (Δ_x, Δ_y) represent the sensor sample spacing in the (x,y) domain. In the adaptive filtering approach, a solution for the impulse response h_{mn} from the knowledge of $f_m(x_i, y_j)$

and $f_b(x_i, y_j)$, call it $\hat{h}_{mn}$, is obtained via minimizing the error function

$$\sum_i \sum_j \mid f_b(x_i, y_j) - \sum_{m=-n_x}^{n_x} \sum_{n=-n_y}^{n_y} \hat{h}_{mn}\ f_m(x_i - m\Delta_x, y_j - n\Delta_y) \mid^2.$$

The resultant solution is used to estimate $f_b(x_i, y_j)$ via

$$\hat{f}_b(x_i, y_j) \equiv \sum_{m=-n_x}^{n_x} \sum_{n=-n_y}^{n_y} \hat{h}_{mn}\ f_m(x_i - m\Delta_x, y_j - n\Delta_y). \tag{3}$$

The statistic used for detecting the moving target is constructed via

$$\hat{f}_d(x_i, y_j) \equiv f_b(x_i, y_j) - \hat{f}_b(x_i, y_j). \tag{4}$$

In the one-dimensional problems, the solution for $\hat{h}_m$ is formed via computing the inverse of a large covariance matrix, a recursive LMS (gradient descent adaptive) algorithm [wid]. These methods may be utilized in the two-dimensional problems via, e.g., *reshaping* the two-dimensional arrays into one-dimensional arrays. This, however, requires processing very large matrices, especially for the covariance matrix and the reshaped discrete filter.

B. Signal Subspace Processing

The signal $\hat{f}_b(x_i, y_j)$ is the projection of $f_b(x_i, y_j)$ into the linear subspace which is defined by $f_m(x_i, y_j)$ and $N - 1$, where $N = N_x N_y$, of its shifted versions; i.e.,

$$\Psi \equiv [\ f_m(x_i - m\Delta_x, y_j - n\Delta_y);\ m = -n_x, \ldots, n_x,\ n = -n_y, \ldots, n_y\ ]$$

Thus, it is sufficient to identify the signal subspace Ψ, and then obtain the projection of $f_b(x_i, y_j)$ into this signal subspace to construct $\hat{f}_b(x_i, y_j)$. Let $\psi_\ell(x_i, y_j)$, $\ell = 1, 2, \ldots, N$, be a set of orthogonal basis functions which spans the linear signal subspace of Ψ. To generate this signal subspace, one can use Gram-Schmidt, modified Gram-Schmidt, Householder or Givens orthogonalization procedure. The size of the signal subspace, i.e., N, depends on the user's a priori knowledge of the number of the nonzero coefficients in the discrete model of the impulse response $h(x, y)$. For instance, if the discrete $h(x, y)$ contains (N_x, N_y) non-zero pixels, then we should select $N = N_x N_y$. In practice, the exact value of $N_x N_y$ is not known. In this case, an estimate should be used based on the maximum anticipated degree of shift and calibration errors between the two sensors.

The projection of the $f_b(x_i, y_j)$ into the basis function $\psi_\ell(x_i, y_j)$, which is identified by the series coefficient a_ℓ ($\ell = 1, 2, \ldots, N$), is found via the following:

$$a_\ell \equiv < \ f_b \ , \ \psi_\ell \ > = \sum_i \sum_j \ f_b(x_i, y_j) \ \psi_\ell^*(x_i, y_j) \tag{5}$$

The projection of $f_b(x_i, y_j)$ into the signal subspace Ψ is

$$\hat{f}_b(x_i, y_j) \equiv \sum_{\ell=1}^{N} \ a_\ell \ \psi_\ell(x_i, y_j). \tag{6}$$

The signal subspace difference image, i.e., the statistic for detecting moving targets is $\hat{f}_d(x_i, y_j)$ in (4). Note that both the adaptive filtering method in [wid] and the signal subspace projection of (5)-(6) seek the same *minimum error energy* solution for the estimate of $f_b(x_i, y_j)$ in the linear subspace of $f_m(x_i, y_j)$ and its shifted versions.

C. Block-Based Processing

Provided that the calibration error function is invariant in the target's coordinates, then the subspace processing can be applied in one step to the entire SAR scene. However, in most wide-angle FOPEN SAR or high-resolution X band SAR systems, the calibration error function cannot be modeled to be invariant in the target's coordinates. In this case, the SAR image has to be divided into subpatches over which the error function does not vary significantly (which implies that $h(x, y)$ approximately remains the same in that subpatch.) The subspace algorithm can then be applied to each subpatch. We refer to this scheme as*block-based* signal subspace processing.

The signature of a moving target commonly appears as a relatively long streak in reconstructed SAR images. As a result, such a signature may be observable in more than one of the subpatches (blocks) where the signal subspace processing is performed. In this case, the signal subspace difference signal $\hat{f}_d(x_i, y_j)$ in (4) indicates the presence of a moving target in all of those subpatches. However, since the model in (2) is being violated (due to the presence of a moving target) differently in each of these subpatches, the signal subspace difference signal $\hat{f}_d(x_i, y_j)$ could exhibit discontinuities or *blocking effect* at the boundaries of the subpatches [s00]. This phenomenon has also been observed in the block-based image compression methods.

The blocking effect is an undesirable artifact in image compression problems since the end product in these problems is the original image. However, in MTD along-track

monopulse SAR, the user is only interested in an indicator, i.e., signal subspace difference signal $\hat{f}_d(x_i, y_j)$, that warns him of the presence of a moving target; the *appearance* of this indicator has no significance. Yet, it is possible to remove the blocking effect and provide a more natural-looking MTI signal. One possible solution for this is to perform signal subspace processing on *overlapping* subpatches, and accumulate the results. The approach is similar to performing a two-dimensional convolution on an image; i.e., a specific operation is performed on the image within a sliding window (subpatch). The results that are provided in this report are based on the overlapping block-based processing. The main shortcoming of this method is its computational cost. (As we noted earlier, if the user is only interested in detecting moving targets, there is no need to use overlapping blocks.)

D. Results

The X band SAR data were collected at the spotlight-mode. The data were collected over a 5-sec slow-time interval within an approximate bandwidth of 600 MHz. The range and cross-range resolution of the system is approximately 30 cm by 30 cm. The imaging scene contains stationary and moving targets on a clear land and roads that are surrounded by relatively dense trees.

Figure 1a shows the SAR reconstruction of a target area that is formed with the monostatic (Channel 1) data of the along-track monopulse SAR system; the imaging scene is composed of a stationary vehicle and one or more moving vehicles on a clear land. (We will discuss the number of moving targets in this scene later.) Figure 1b is the close-up of the stationary vehicle in this target area. The reconstruction of this scene from the bistatic (Channel 2) data resembles the image in Figure 1a; this is not presented.

A common and simple way to calibrate the monostatic and bistatic SAR images is to model their relationship via a constant phase and a constant gain; i.e.

$$f_b(x_i, y_j) = h_{00}\ f_m(x_i, y_j), \tag{7}$$

where h_{00} is an unknown complex constant (representing the gain and phase difference between the monostatic and bistatic SAR images). Note that the model in (7) is a special case of the general miscalibration model in (2) with $n_x = n_y = 0$. Provided that the model in (7) is true, the LMS estimate (projection) of $f_b(x_i, y_j)$ into signal subspace of $f_m(x_i, y_j)$ is achieved via

$$\hat{f}_{b0}(x_i, y_j) = \frac{E_{bm}}{\sqrt{E_b\ E_m}}\ f_m(x_i, y_j), \tag{8}$$

where

$$E_{bm} \equiv < \ f_b \ , \ f_m \ >, \tag{9}$$

is the cross-correlation between the monostatic and bistatic SAR images, and E_b and E_m are the energies of the bistatic and monostatic SAR images, respectively. Figure 2a is the coherent difference of the monostatic SAR image and estimated bistatic SAR image in (8), i.e.,

$$\hat{f}_{b0}(x_i, y_j) - f_m(x_i, y_j); \tag{10}$$

Figure 2b is the close-up of the stationary vehicle in this image. The figure shows that this static has failed to null the stationary targets.

Due to various sources of phase errors between the two channels of an along-track monopulse SAR system, it has been argued that the *noncoherent* processing of the monostatic and bistatic SAR images in the above-mentioned procedure would result in a more reliable MTI statistic. For this the cross-correlation is recomputed as

$$E_{bm} \equiv < \ |f_b| \ , \ |f_m| \ > . \tag{11}$$

After computing the bistatic SAR image projection from (8), the noncoherent difference is found from

$$|\hat{f}_{b0}(x_i, y_j)| - |f_m(x_i, y_j)|. \tag{12}$$

Figure 3a shows this MTI image; Figure 3b is the close-up of the stationary vehicle in this image. This noncoherent MTI statistic also fails to null the stationary targets.

Figure 4a shows the overlapping block-based signal subspace difference image (see (4)); Figure 4b is the close-up of the stationary vehicle in this image. To generate this signal subspace difference image, we use 20 pixels by 20 pixels blocks (approximately 5 m by 5 m), and a filter size of 3 pixels by 3 pixels. The vertical *streaks* in Figure 4a represent the signature of the moving targets. Note that some of these streaks (i.e., moving target signatures) are not visible in the original SAR reconstruction of Figure 1a. While the signature of the stationary vehicle is not completely nulled in the signal subspace MTI statistic in Figure 4b, it is relatively weak with respect to the moving targets signatures.

To demonstrate this, consider the distributions in the range domain in Figure 5. The dashed line in Figure 5a is the distribution of the monostatic SAR image (see Figure 1a) in the range domain at the peak point of this image that is located at the azimuth $y = -37.6$

m; the peak is the signature of the stationary vehicle. The solid line in Figure 5a is the distribution of the signal subspace difference image (see Figure 4) in the range domain at the same azimuth $y = -37.6$ m; the stationary target signature is mainly suppressed in this distribution.

In Figure 5b, similar distributions in the range domain are shown at the peak point of the signal subspace difference image (i.e., Figure 4a) that is located at the azimuth $y = 22.45$ m; the peak is the signature of a moving vehicle. Note that the signature of the moving vehicle is not nulled after signal subspace difference processing.

Figure 6a shows the SAR reconstruction of another target area that is obtained with the monostatic (Channel 1) data of the along-track monopulse SAR system; the target area is composed of a foliage region with moving targets in its surroundings. The reconstruction from the bistatic (Channel 2) data resembles the image in Figure 3a, and is not shown here. Figures 6b and 6c are, respectively, coherent difference (see (10)) and noncoherent difference (see (12)); neither of these two statistic result in nulling of the foliage in the imaging scene. Figure 6d shows the overlapping block-based signal subspace difference image. The vertical streaks in this figure represent the signature of the moving targets.

To demonstrate the signal levels in these images, we consider their distributions in the range domain. Figures 7a and 7b, respectively, are these distributions at the peak points of the monostatic SAR reconstruction (Figure 6a), that is at the azimuth $y = 58.26$ m, and the signal subspace difference image (in Figure 6d), that is at the azimuth $y = -8.14$ m. These distributions indicate that the signature of moving targets are below the foliage signature in the formed SAR image. However, the signatures of the moving targets become more prominent than the signature of the foliage in the signal subspace difference image.

5. Motion Estimation and Moving Target Imaging

A. SAR Signal Model for a Moving Target

In our discussion of moving target detection using an along-track monopulse SAR, we did not impose any restrictions on the length of the slow-time processing, and did not restrict the target motion to be linear. In fact, this MTD system could be more effective with a longer slow-time processing (since the probability of recording the moving target SAR signature at its "flash" angles increases). Moreover, a target with a nonlinear motion and/or maneuvering motion model is more likely to cause a more significant phase

difference between the monopulse channels that is useful for MTD [s99a].

Once a moving target is detected, our next task is to estimate its motion track and perhaps image the target; this problem is analogous to Inverse SAR (ISAR) imaging of airborne targets [s94]. For this task, however, the target motion model and the length of the slow-time processing do play restrictive roles. For example, tracking and imaging a maneuvering target with a nonlinear motion on the ground over a relatively long slow-time interval is likely to be infeasible; this is due to the *movement* (not related to the target motion) of its scattering centers as the radar aspect angle varies. (There are also problems associated with terrain variations, etc.)

To show this phenomenon, we divide the synthetic aperture data that are used to form the image in Figure 1a into four disjoint subapertures (i.e., each subaperture is over 1.25 sec of slow-time processing). Figure 8a shows the resultant four subaperture reconstructions. Figure 8b are the close-ups of the stationary vehicle in these four reconstructions. Note the variations of the vehicle dominant scatterers (scattering centers) with respect to the subapertures. We can also note more dramatic variations in the signatures of the moving targets in the four subaperture reconstructions of Figure 8a.

Thus, if there is to be an imaging component in our problem, it has to be formulated over relatively "small" slow-time intervals (subapertures) over which a simpler motion and target model can be used; one may select these subapertures in an overlapping fashion to track the target, e.g., see the discussion on ISAR problem for a maneuvering target in [s94, Sec. 5.6]. To start, one can use a simple constant velocity model in the slant-range and cross-range domains (during a slow-time subaperture). The analysis that follows is based on this.

We denote the speed of the airborne aircraft which carries the radar with v_r, and the slow-time domain by $\tau = \frac{u}{v_r}$, where u is the synthetic aperture domain. Suppose the velocity vector for the n-th target is (v_{xn}, v_{yn}) in the spatial (x, y) domain which is unknown; and let the coordinates of the n-th target at the slow-time zero be (x_n, y_n). In this case, the SAR signature of the n-th target in the fast-time frequency ω domain and synthetic aperture (slow-time) u domain can be shown to be [s99b]

$$s_n(\omega, u) = \exp\big[\, -j2k \sqrt{(x_n - v_{xn}\,\tau)^2 + (y_n - v_{yn}\,\tau - v_r\,\tau)^2}\,\big] \tag{13}$$

where $k = \omega/c$ is the wavenumber. The model in (13) can be written in the following form [s95], [s99b]:

$$s_n(\omega, u) = \exp\big[\, -j2k\, \sqrt{\mathbf{X}_n^2 + (\mathbf{Y}_n - \alpha_n u)^2}\big], \tag{14}$$

where

$$\alpha_n = \frac{\sqrt{v_{xn}^2 + (v_{yn} + v_r)^2}}{v_r}, \tag{15}$$

and

$$\begin{bmatrix} \mathbf{X}_n \\ \mathbf{Y}_n \end{bmatrix} = \begin{bmatrix} \cos\theta_n & \sin\theta_n \\ -\sin\theta_n & \cos\theta_n \end{bmatrix} \begin{bmatrix} x_n \\ y_n \end{bmatrix}, \tag{16}$$

with

$$\theta_n = \arctan\left(\frac{v_{xn}}{v_{yn} + v_r}\right). \tag{17}$$

We call $(\mathbf{X}_n, \mathbf{Y}_n)$ the motion-transformed coordinates of the n-th target; the parameter α_n is the relative speed of the n-th target with respect to the radar.

B. SAR Ambiguity Function for Estimating Speed

The classical radar problem of detecting and estimating the range and speed of a moving target in the one-dimensional spatial domain is based on a two-dimensional reconstructed image or ambiguity function in the (x, v_x) domain [van]; x and v_x, respectively, are the target range and speed in the range domain. The basic approach is to develop a two-dimensional statistic, which is called the *ambiguity function*, to determine the range coordinates and speed values of moving targets in the irradiated target scene.

The analogous problem which we encounter in SAR is to detect and estimate the location and velocity of a moving target in the two-dimensional (slant-range and cross-range) domain. One may intuitively rationalize that this SAR problem requires a four-dimensional reconstructed image or ambiguity function in the (x, y, v_x, v_y) domain. However, in eqs. (14)-(17) we showed that whether a target in a SAR scene is stationary or moving, its *relative* motion trajectory with respect to the radar can be modeled by at most three parameters. This leads to a simpler approach to first estimate a target's motion parameter, and then use the outcome to image that target [s95], [s99b].

The first step of this approach is to construct a SAR ambiguity function that provides the user with the relative speed of a moving target (e.g., α_n for the n-th target model in (14)) that has been detected by the subspace difference signal $\hat{f}_d(x_i, y_j)$. The subspace difference signal identifies the region in the spatial domain where the moving targets' signatures are located at. For instance, Figure 4a shows that the moving target region is around the range interval of $x_i \in [8, 12]$ m, and the cross-range interval of $y_j \in [-30, 50]$ m. (Note that in this scenario the moving targets are on a clear land, and are not surrounded by foliage.) Next, the same region is identified in the reconstructed monostatic (or bistatic)

image $f_m(x_i, y_j)$ in Figure 1a. (Clearly, the signature of the moving targets are smeared in this image; however, this has no impact on the operations that follow.)

We identify the small region around the above coordinates where the *smeared* signature of the n-th target appears as $\mathbf{R}_n$. Thus, we can approximately reconstruct the measured SAR signature of the n-th target in the (ω, u) domain via the following:

$$s_n(\omega, u) \approx \sum_{(x_i, y_j) \in \mathbf{R}_n} f_m(x_i, y_j) \; \exp\left[-j2k\sqrt{x_i^2 + (y_j - u)^2}\right]. \tag{18}$$

Note that $f_m(x_i, y_j)$, $(x_i, y_j) \in \mathbf{R}_n$, represent the *coherent* (complex) values of the monostatic SAR reconstruction at the region that the n-th target signature appears We identify the above estimate of the target signature $s_n(\omega, u)$ as the *digitally-spotlighted* SAR signature of the region $\mathbf{R}_n$ in the reconstructed image. (One may also construct $s_n(\omega, u)$ via the inverse of the SAR wavefront reconstruction, that involves various FFTs and inverse of the Stolt interpolation.)

Construction of an ambiguity function in SAR that provides the user with information of a moving target relative speed is based on the observation that the n-th target signature in (14) is a phase-modulated signal that approximately contains a chirp-type function of the form [s95]

$$\exp\left(j \; \frac{k \; \alpha_n^2 \; u^2}{r_n}\right),$$

where r_n is the mean radial range of the digitally-spotlighted area. Next, we mix the n-th moving target signature with the complex conjugate of this class of chirp signals at various scales (i.e., α values):

$$\gamma_n(\omega, u, \alpha) = s_n(\omega, u) \; \exp\left(-j \; \frac{k \; \alpha^2 \; u^2}{r_n}\right). \tag{19}$$

(Ref. [s99b] provides a more elaborate expression and analysis of this processing.) We identify the Fourier transform of the signal in (19) with respect to the synthetic aperture u via

$$\Gamma_n(\omega, k_u, \alpha) = \mathcal{F}_{(u)} \left[\; \gamma_n(\omega, u, \alpha) \; \right]. \tag{20}$$

We call the signal $\Gamma_n(\omega, k_u, \alpha)$ the *SAR ambiguity function* that can be used to estimate the relative speed of a moving target. The reason for this is described below.

Suppose the signature which appears at the region $\mathbf{R}_n$ belongs to a target with a relative speed of α_n. In this case,, at a fixed fast-time frequency ω, the SAR ambiguity

function $\Gamma_n(\omega, k_u, \alpha)$ exhibits a sharp peak in the (k_u, α) domain around $\alpha = \alpha_n$. Moreover, as α moves away from the target relative speed α_n, the SAR ambiguity function $\Gamma_n(\omega, k_u, \alpha)$ becomes weaker and more spread (smeared) [s95]. Note that the SAR ambiguity function $\Gamma_n(\omega, k_u, \alpha)$ is a three-dimensional signal. However, one needs only to form the SAR ambiguity function at one of the fast-time frequencies of the radar signal, that is, a fixed ω to estimate α_n

Figure 9 shows the SAR ambiguity function at the carrier frequency for the digitally-spotlighted signature of the moving target region of Figure 1a, i.e., the range interval of $x_i \in [8, 12]$ m, and the cross-range interval of $y_j \in [-30, 50]$ m. This ambiguity function shows *two* distinct peak regions: one is centered around $\alpha = 1.1175$ (approximately 15 m/sec), and the other is around $\alpha = 1.0475$ (approximately 6 m/sec). Based on this observation, one can conclude that either there are at least two moving targets in the scene, or a moving target has changed its speed during the data acquisition. The latter scenario is unlikely since such a signature would exhibit a "connection" between the two peaks. (The two peaks in Figure 9 are disjoint and isolated.) Note that the peak at $\alpha = 1.1175$ is relatively sharp; this indicates a target that is moving with a relatively constant velocity. However, the peak at $\alpha = 1.0475$ seems more chaotic (not localized) that could be due maneuvering and/or acceleration/deacceleration of the moving target. (This will become more evident in the results of imaging these targets in the next section.)

We next turn our attention to the moving targets around the foliage area in Figure 6a, and their signal subspace difference image in Figure 6d. Unlike the case of the moving targets on the clear land, the desired moving target signature in Figure 6a overlaps with the signature of the foliage in the area. Thus, after detecting a moving target using the signal subspace difference of Figure 6d, the user may use a smaller region of the spatial domain for digital-spotlighting. For instance, we use the range interval of $x_i \in [5, 10]$ m, and the cross-range interval of $y_j \in [15, 25]$ m that appears to have a weak foliage signature. The SAR ambiguity function for this area is shown in Figure 10; the peak of this distribution is around $\alpha = .9258$ (approximately 10 m/sec). Note that the distribution is not localized; as we mentioned earlier, this could be due the maneuvering and/or acceleration/deacceleration of the moving target. We constructed the ambiguity function for the other segments of the moving target signature in Figure 6a. The results show variations of the relative speed near $\alpha = .92$. This is likely due to the presence of several moving targets (a convoy) at slightly different speed values.

C. Moving Target Imaging

The SAR reconstruction of a moving target appears smeared and shifted if it is treated as a stationary target [s94]. However, the reconstruction of a moving target is focused if the value of its relative speed α is incorporated into the reconstruction algorithm. The SAR imaging of a scene which is composed of moving targets as well as stationary targets can be formulated as a three-dimensional imaging in the $(\mathbf{X}, \mathbf{Y}, \alpha)$ domain. The three-dimensional reconstruction in what we refer to as the motion-transformed spatial domain $(\mathbf{X}, \mathbf{Y})$ and the relative speed domain α can be achieved via the following [s99b].

We denote the two-dimensional Fourier transform of the measured SAR data with $S(\omega, k_u)$. Then, the reconstruction equation in the spatial frequency domain of $(\mathbf{X}, \mathbf{Y})$ for targets with relative speed α is

$$\mathbf{F}(k_{\mathbf{X}}, k_{\mathbf{Y}}, \alpha) = S(\omega, k_u), \tag{21}$$

where

$$\begin{aligned} k_{\mathbf{X}} &= \sqrt{4k^2 - \left(\frac{k_u}{\alpha}\right)^2} \\ k_{\mathbf{Y}} &= \frac{k_u}{\alpha} \end{aligned} \tag{22}$$

The inverse two-dimensional Fourier transform of this signal with respect to $(k_{\mathbf{X}}, k_{\mathbf{Y}})$

$$\mathbf{f}(\mathbf{X}, \mathbf{Y}, \alpha) = \mathcal{F}^{-1}_{(k_{\mathbf{X}}, k_{\mathbf{Y}})} \Big[\mathbf{F}(k_{\mathbf{X}}, k_{\mathbf{Y}}, \alpha) \Big]$$

is representative of targets with relative speed α *in focus.*

Figure 11a shows the reconstruction of the imaging scene of Figure 1a (that is formed with $\alpha = 1$) using $\alpha = 1.1175$; this is one of the peak points in the SAR ambiguity function of Figure 9. The reconstruction in Figure 11a shows a focused target; the close-up of this focused target is shown in Figure 11b. Recall that the SAR ambiguity of this target in Figure 9 is relatively localized, and its SAR image is also fairly focused in Figure 11b.

Similar results for the targets on the clear land using $\alpha = 1.0475$ are shown in Figures 12a and 12b. Note that for this moving target, the SAR ambiguity function in Figure 9 is not localized, and its SAR image in Figure 12b appears more smeared than the image of the first moving target in Figure 11b. The moving target imaging result for the target (or targets) with $\alpha = .9258$ near the foliage region (i.e., the peak point in the SAR ambiguity distribution in Figure 10) is shown in Figure 13. Note that this image shows two targets

at $(x, y) \approx (8, 7)$ m and $(x, y) \approx (27, 47)$ m; these two moving targets are not as focused as the target in Figure 11b.

Our final example involves a maneuvering target with *slow* motion components that are nonlinear. The reconstructed image of this target with $\alpha = 1$ is shown in Figure 14a. The SAR ambiguity function of this target exhibits a chaotic behavior around $\alpha = .98$ (approximately 2.5 m/sec); this is not shown here. Imaging using $\alpha = .98$ would not result in a significant improvement (focusing) over the image that is shown in Figure 14a. As an alternative, we apply a motion compensation method that we have developed for ISAR imaging of aircrafts; this algorithm attempts to solve for the target nonlinear motion in the slow-time domain. The motion-compensated image is shown in Figure 14b.

6. Conclusions

This report presented moving target detection and imaging results for an X band along-track monopulse SAR system. A signal subspace processing was used to blindly calibrate the two channels of the monopulse SAR system. This helped us to construct an MTI statistic that suppresses the stationary background. Once a moving target was detected, its speed was estimated using its SAR ambiguity function. The estimated speed was then used to image the moving target under a constant velocity approximation. The method was shown to be fairly effective in providing a focused image of a moving target whose SAR ambiguity signature was localized. The results were also shown for other moving targets whose motion might contain nonlinear and/or maneuvering components.

7. References

[can] B. Cantrell, "A short-pulse area MTI," NRL Report 8162, September 1977.

[che] H. Chen and C. McGillem, "Target motion compensation by spectrum shifting a synthetic aperture radar," *IEEE Transactions on Aerospace and Electronic Systems,* pp. 895-900, July 1992.

[kir] J. Kirk, "Motion compensation for synthetic aperture radar," *IEEE Transactions on Aerospace and Electronic Systems,* pp. 338-348, May 1975.

[leo] A. Leonov and K. Fomichev, *Monopulse Radar*, Translated by W. Barton, Artech House 1986.

[mar] P. Marques and J. Dias, "Efficient detection and ground mapping of selected moving targets using SAR raw-data," in *Proceedings of IGARSS '99,* Hamburg, Germany, June 1999.

[per] R. Perry, R. Dipietro and R. Fante, "SAR imaging of moving targets," *IEEE Transactions on Aerospace and Electronic Systems,* vol. 35, pp. 188-200, January 1999.

[ran] R. Raney, "Synthetic aperture imaging radar and moving targets," *IEEE Transactions on Aerospace and Electronic Systems,* vol. 7, pp. 499-505, 1971.

[rao] R. Rao and P. Mahapatra, "Imaging of moving targets using squint mode SAR," in *Proceedings of EUSAR 2000,* pp. 553-556, Munich, Germany, May 2000.

[she] S. Sherman, *Monopulse Principles and Techniques,* Artech House, 1984.

[van] H. Van Trees, *Detection, Estimation, and Modulation Theory,* vol. III, New York: Wiley, 1968.

[wid] B. Widrow, *Adaptive Signal Processing,* Englewood Cliffs, NJ: Prentice Hall, 1985.

[yan] H. Yang and M. Soumekh, "Blind-velocity SAR/ISAR imaging of a moving target in a stationary background," *IEEE Transactions on Image Processing*, vol. 2, pp. 80-95, January 1993.

[s94] M. Soumekh, *Fourier Array Imaging*, Englewood Cliffs, NJ: Prentice Hall, 1994.

[s95] M. Soumekh, "Reconnaissance with ultra wideband UHF synthetic aperture radar," *IEEE Signal Processing Magazine*, vol. 12, no. 4, pp. 21-40, July 1995.

[s97] M. Soumekh, "Moving target detection in foliage using along track monopulse synthetic aperture radar imaging," *IEEE Transactions on Image Processing*, vol. 6, no. 8, pp. 1148-1163, August 1997.

[s99a] M. Soumekh, "Signal subspace fusion of uncalibrated sensors with application in SAR and diagnostic medicine," *IEEE Transactions on Image Processing*, vol. 8, no. 1, pp. 127-137, January 1999.

[s99b] M. Soumekh, *Synthetic Aperture Radar Signal Processing with MATLAB Algorithms*, New York: Wiley, 1999.

[s00] M. Soumekh, S. Sworrell, E. Zelnio and B. Keaffaber, "SAR wavefront reconstruction using motion compensated phase history (polar format) data and DPCA-based GMTI," *Proc. of SPIE's Annual International Symposium on Aerospace/Defense Sensing, Simulation, and Controls*, Orlando, April 2000.

8. Figure Captions

1. a) SAR reconstruction of a target area that is formed with the monostatic data of the along-track monopulse SAR system; the imaging scene is composed of a stationary vehicle and one or more moving vehicles on a clear land. b) Close-up of the stationary vehicle in this target area.

2. a) Coherent difference of the monostatic SAR image and estimated bistatic SAR image using (8); see (10). b) Close-up of the stationary vehicle in this image.

3. a) Noncoherent difference of the monostatic SAR image and estimated bistatic SAR image using noncoherent version of (8); see (12). b) Close-up of the stationary vehicle in this image.

4. a) Signal subspace difference image. b) Close-up of the stationary vehicle in this image.

5. a) Dashed line is the distribution of the monostatic SAR image in the range domain at the peak point of Figure 1a that is located at the azimuth $y = -37.6$ m. Solid line is the distribution of the signal subspace difference image in the range domain at the same azimuth. b) Similar distributions as in (a) at the peak point of the signal subspace difference image in Figure 4a that is located at the azimuth $y = 22.45$ m.

6. a) SAR reconstruction of a target area that is formed with the monostatic data of the along-track monopulse SAR system; the imaging scene is composed of a dense foliage area and one or more moving vehicles on the nearby roads. b) Coherent difference of the monostatic SAR image and estimated bistatic SAR image using (8); c) Noncoherent difference of the monostatic SAR image and estimated bistatic SAR image using noncoherent version of (8); d) Signal subspace difference image.

7. a) Dashed line is the distribution of the monostatic SAR image in the range domain at the peak point of Figure 6a that is located at the azimuth $y = 58.26$ m. Solid line is the distribution of the signal subspace difference image in the range domain at the same azimuth. b) Similar distributions as in (a) at the peak point of the signal subspace difference image in Figure 6d that is located at the azimuth $y = -8.14$ m.

8. a) Four subaperture reconstructions of the target area in Figure 1a. b) Close-ups of the stationary vehicle in these four reconstructions.

9. SAR ambiguity function at the carrier frequency for the digitally-spotlighted signature of the moving target region in Figure 1a.

10. SAR ambiguity function at the carrier frequency for the digitally-spotlighted signature of the moving target region in Figure 6a.

11. a) Moving target reconstruction of the imaging scene of Figure 1a using $\alpha = 1.1175$.
    b) Close-up of the focused target in (a).

12. a) Moving target reconstruction of the imaging scene of Figure 1a using $\alpha = 1.0475$.
    b) Close-up of the focused target in (a).

13. Moving target reconstruction of the imaging scene of Figure 6a using $\alpha \doteq .9258$.

14. Reconstruction of maneuvering target: a) $\alpha = 1$ (uncompensated for motion); b) motion-compensated using ISAR processing.

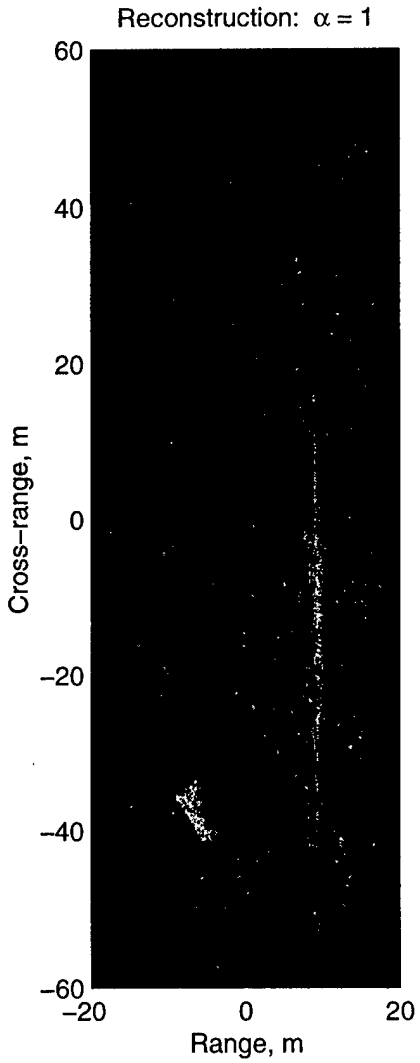
Reconstruction: α = 1
60
40
20
0
−20
−40
−60
Cross−range, m
−20
0
20
Range, m

(a)

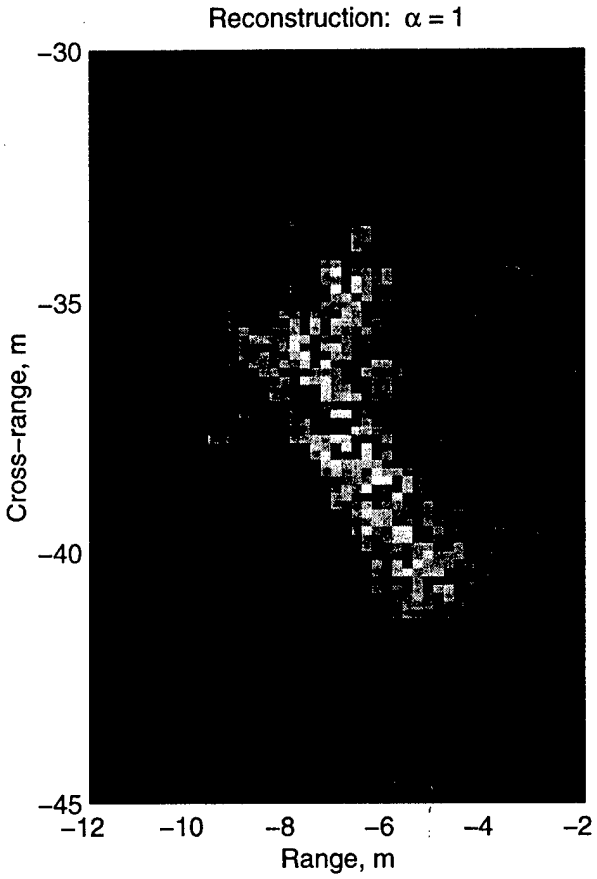
Reconstruction: α = 1
−30
−35
−40
−45
Cross−range, m
−12
−10
−8
−6
−4
−2
Range, m

(b)

Fig. 1

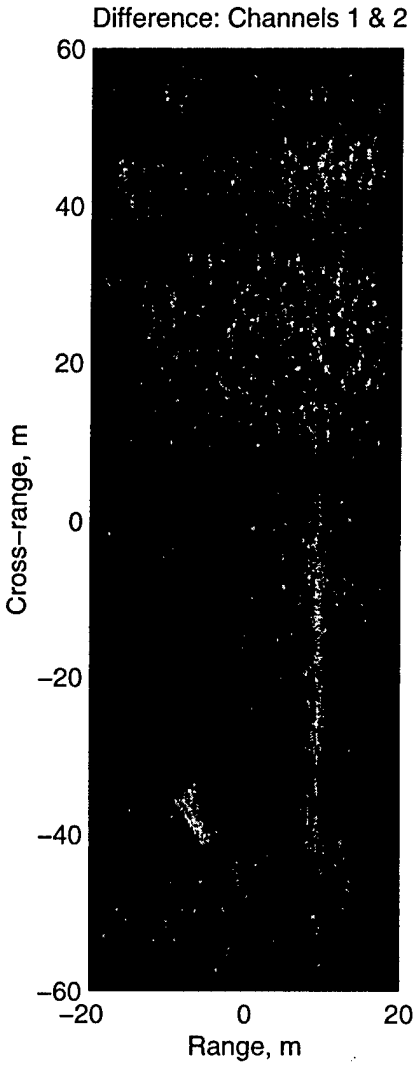
Difference: Channels 1 & 2
60
40
20
0
−20
−40
−60
Cross−range, m
−20
0
20
Range, m

(a)

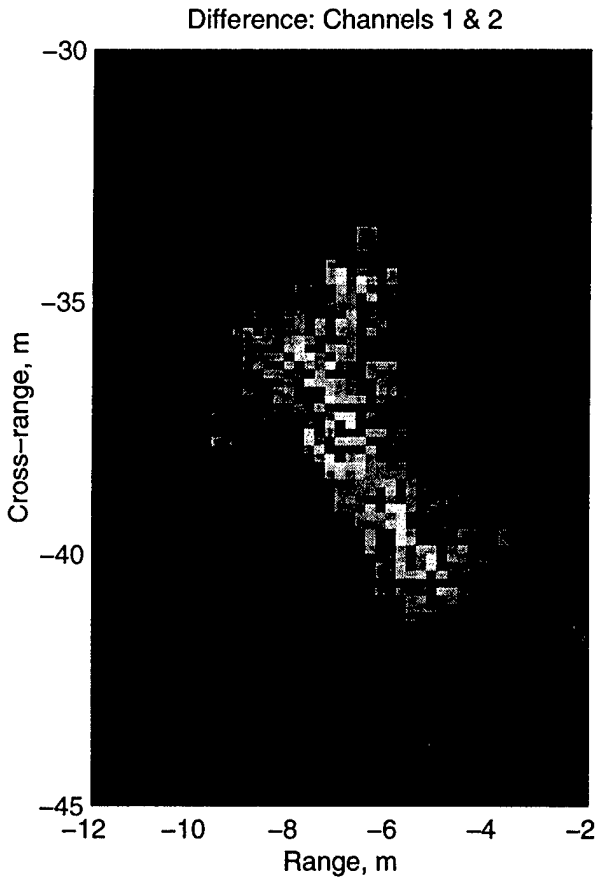
Difference: Channels 1 & 2
−30
−35
−40
−45
Cross−range, m
−12
−10
−8
−6
−4
−2
Range, m

(b)

Fig. 2

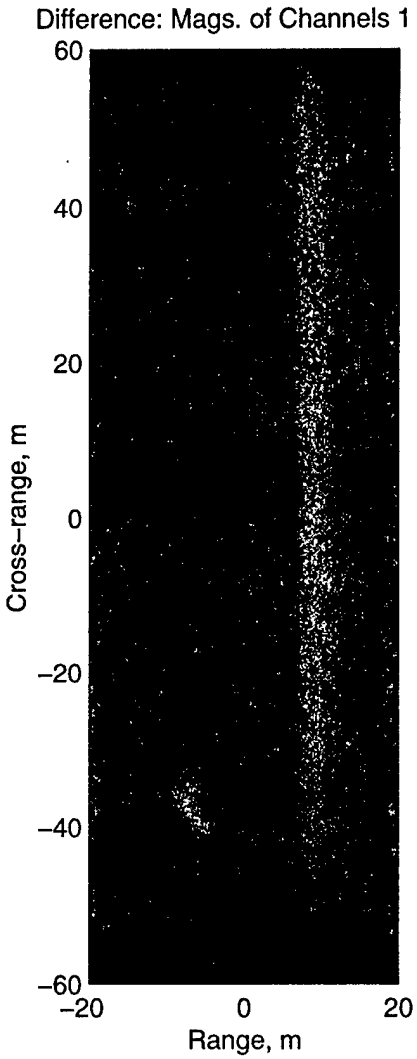
Difference: Mags. of Channels 1 & 2
60
40
20
0
−20
−40
−60
Cross−range, m
−20
0
20
Range, m

(a)

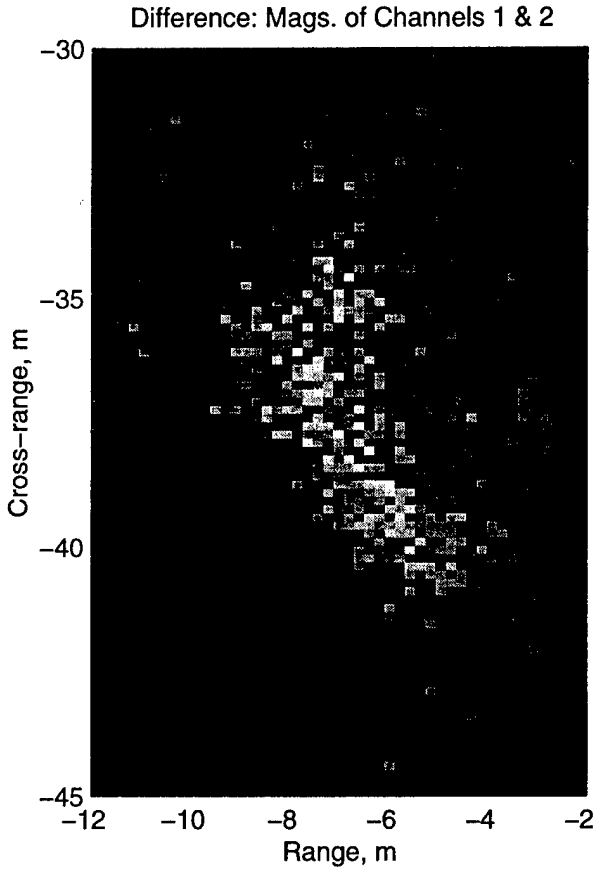
Difference: Mags. of Channels 1 & 2
−30
−35
−40
−45
Cross−range, m
−12
−10
−8
−6
−4
−2
Range, m

(b)

Fig. 3

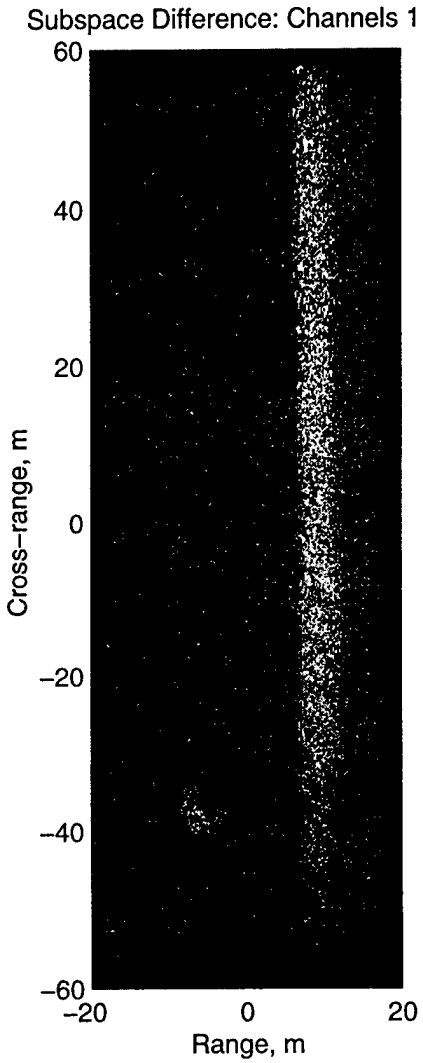
Subspace Difference: Channels 1 & 2
60
40
20
0
−20
−40
−60
Cross−range, m
−20
0
20
Range, m

(a)

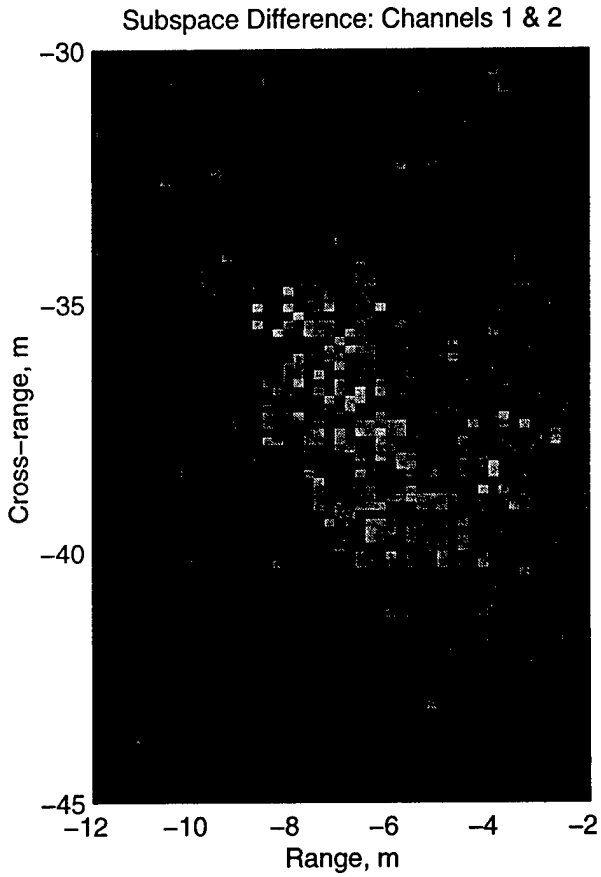
Subspace Difference: Channels 1 & 2
−30
−35
−40
−45
Cross−range, m
−12
−10
−8
−6
−4
−2
Range, m

(b)

Fig. 4

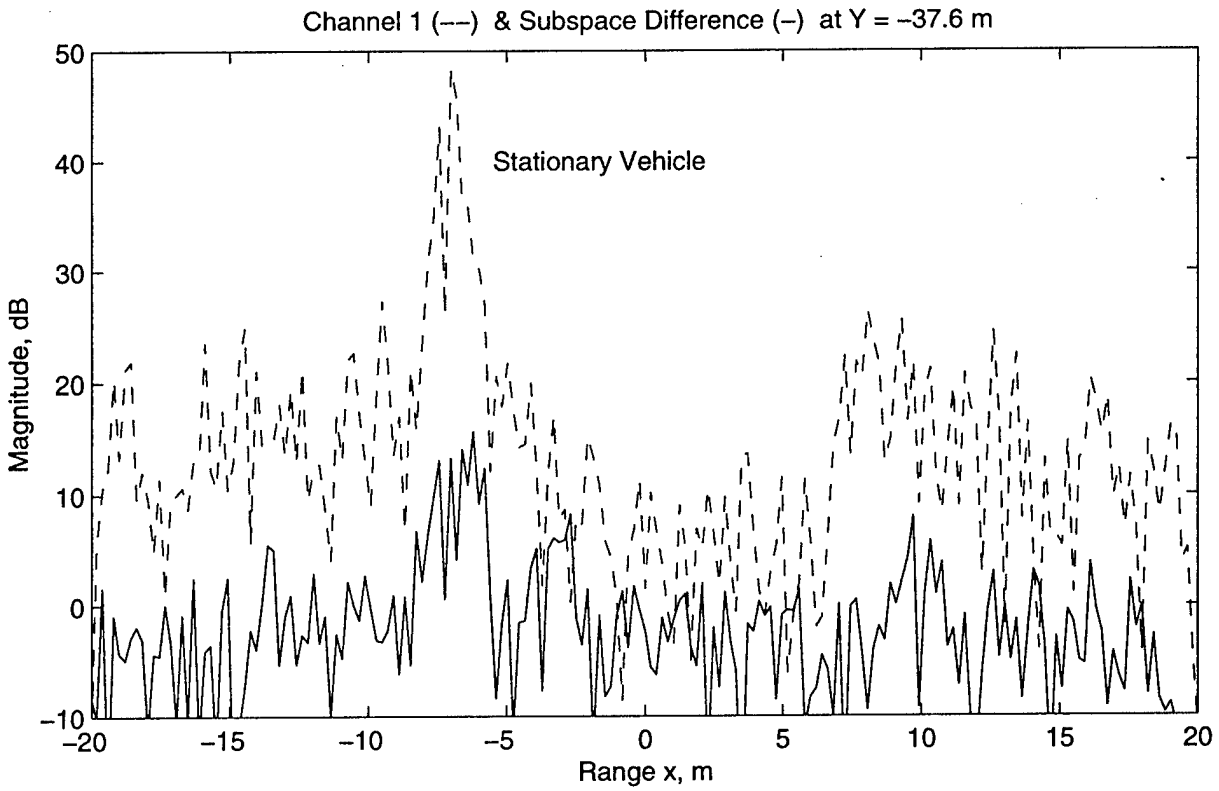
Channel 1 (---) & Subspace Difference (–) at Y = –37.6 m
Stationary Vehicle
Magnitude, dB
Range x, m
50
40
30
20
10
0
–10
–20
–15
–10
–5
0
5
10
15
20

(a)

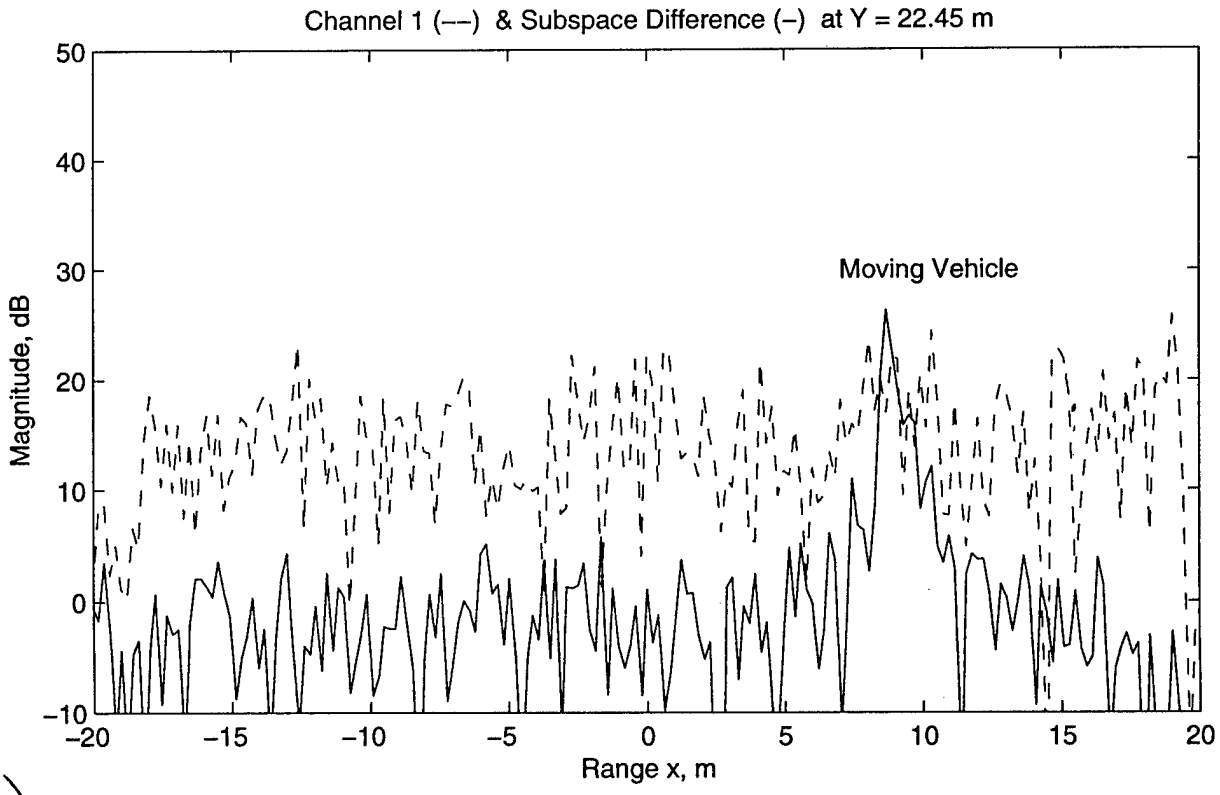
Channel 1 (---) & Subspace Difference (–) at Y = 22.45 m
Moving Vehicle
Magnitude, dB
Range x, m
50
40
30
20
10
0
–10
–20
–15
–10
–5
0
5
10
15
20

(b)

Fig. 5

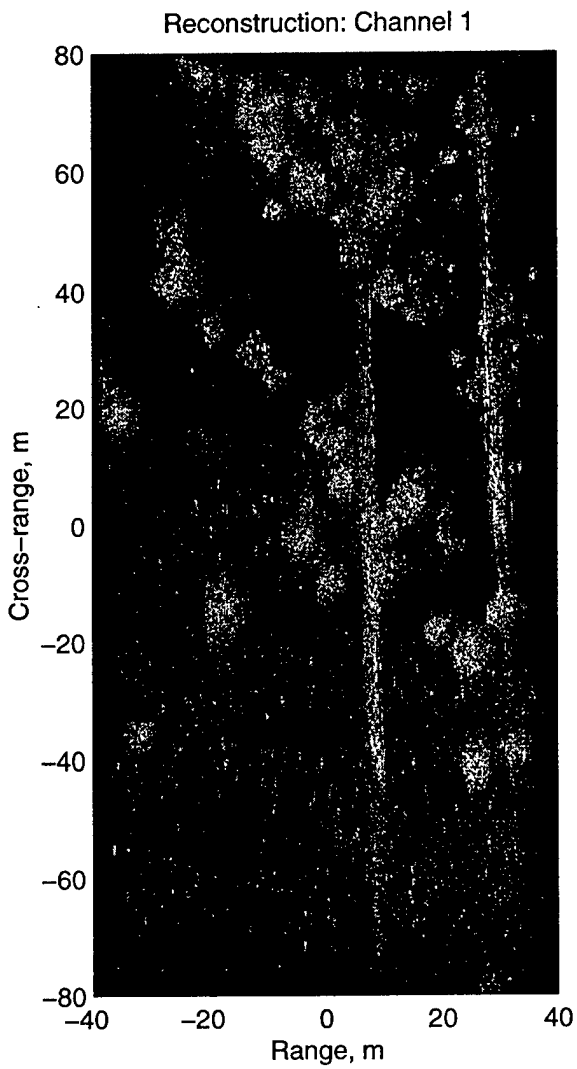
Reconstruction: Channel 1
80
60
40
20
0
−20
−40
−60
−80
Cross−range, m
−40
−20
0
20
40
Range, m

(a)

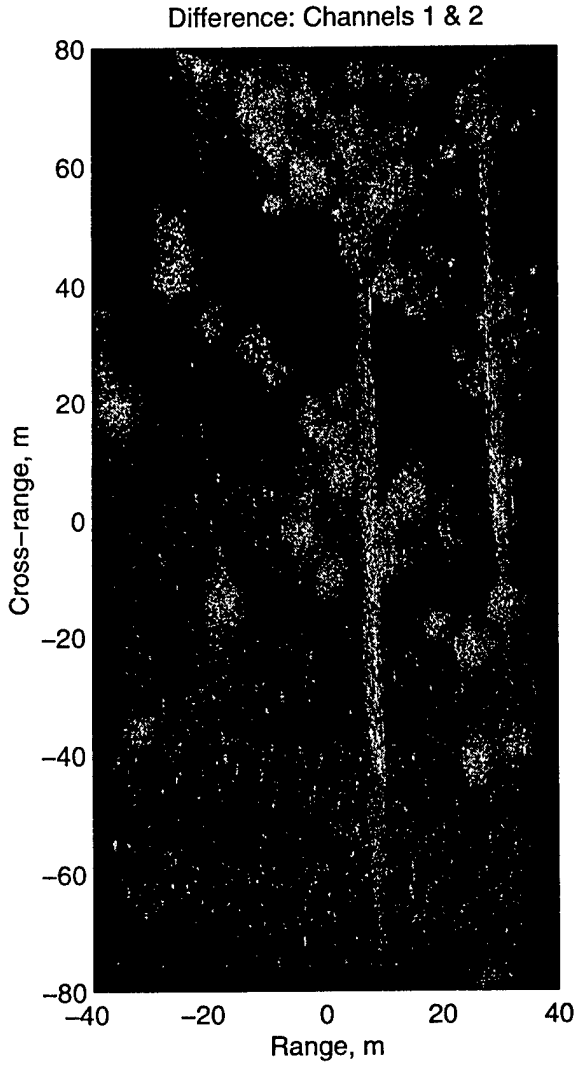
Difference: Channels 1 & 2
80
60
40
20
0
−20
−40
−60
−80
Cross−range, m
−40
−20
0
20
40
Range, m

(b)

Fig. 6

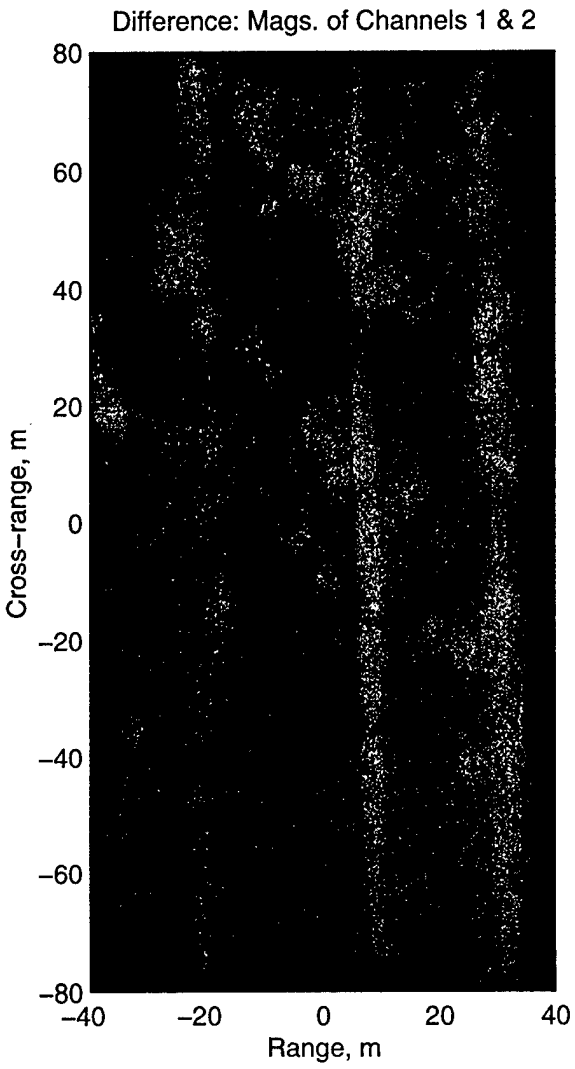
Difference: Mags. of Channels 1 & 2
80
60
40
20
0
−20
−40
−60
−80
Cross−range, m
−40
−20
0
20
40
Range, m

(c)

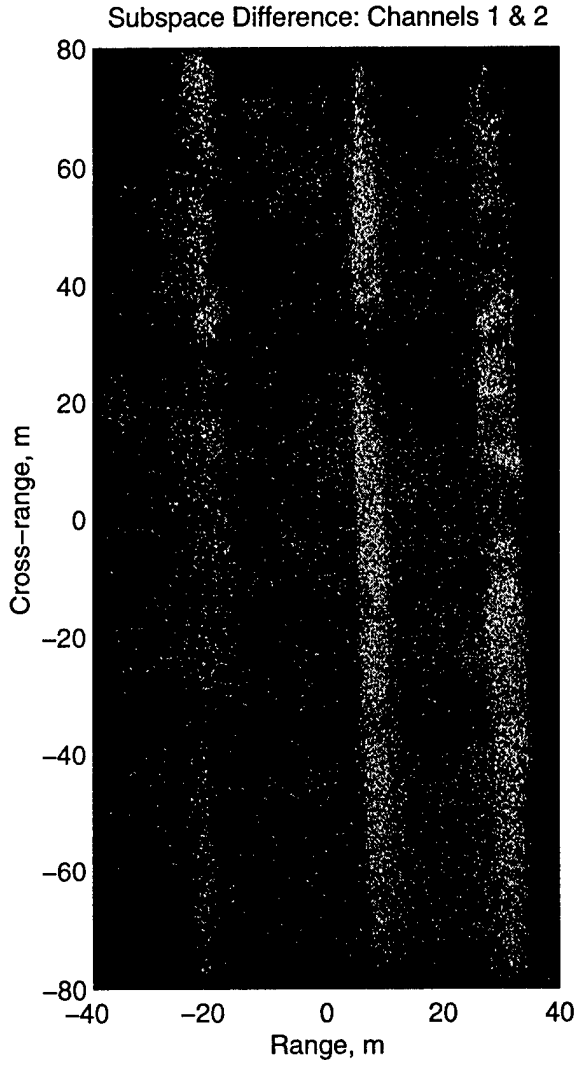
Subspace Difference: Channels 1 & 2
80
60
40
20
0
−20
−40
−60
−80
Cross−range, m
−40
−20
0
20
40
Range, m

(d)

Fig. 6 (cont)

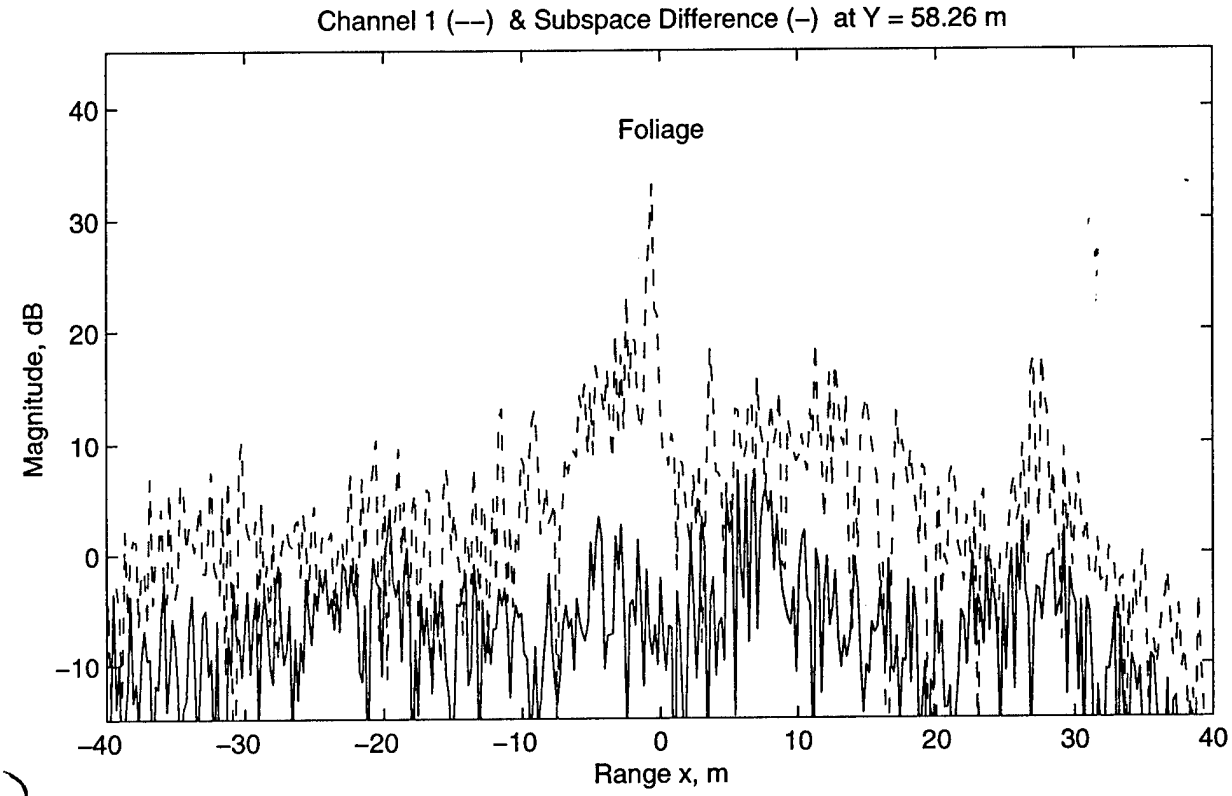
Channel 1 (---) & Subspace Difference (–) at Y = 58.26 m
Foliage
Magnitude, dB
Range x, m
40
30
20
10
0
–10
–40
–30
–20
–10
0
10
20
30
40

(a)

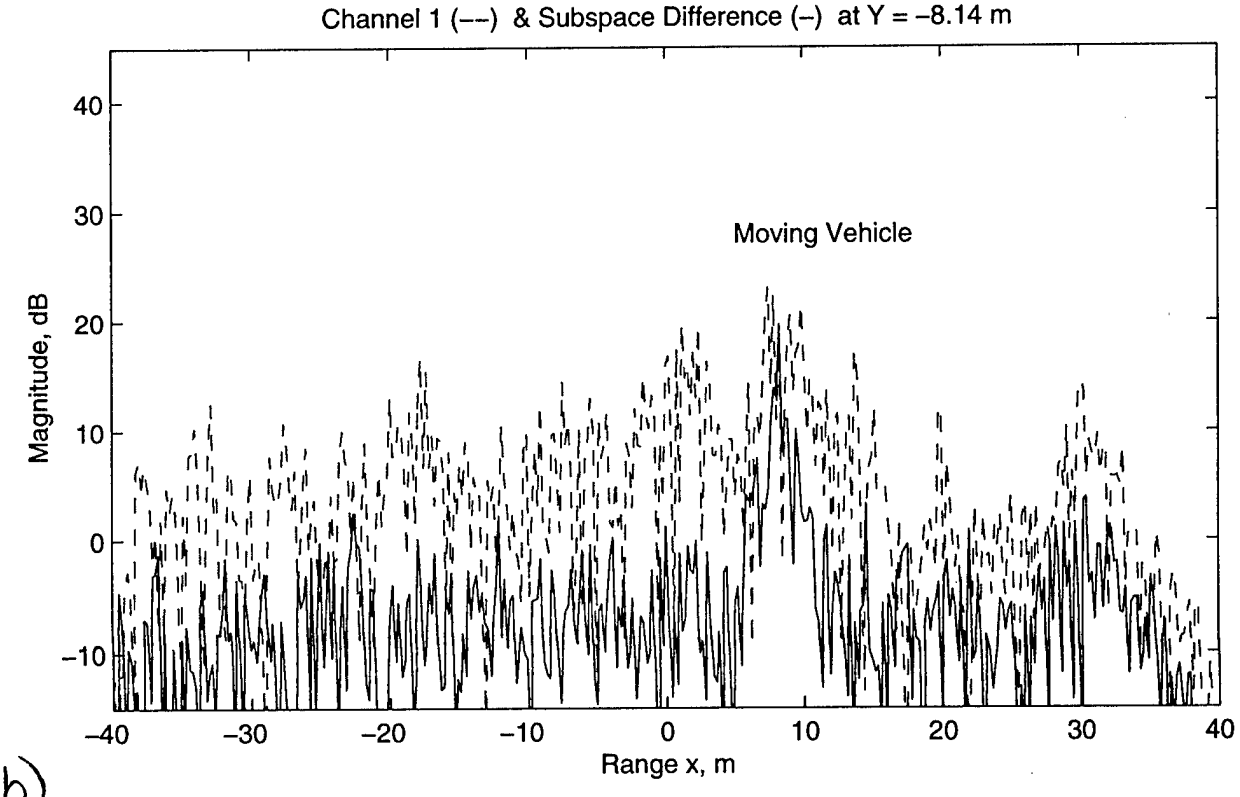
Channel 1 (---) & Subspace Difference (–) at Y = –8.14 m
Moving Vehicle
Magnitude, dB
Range x, m
40
30
20
10
0
–10
–40
–30
–20
–10
0
10
20
30
40

(b)

Fig. 7

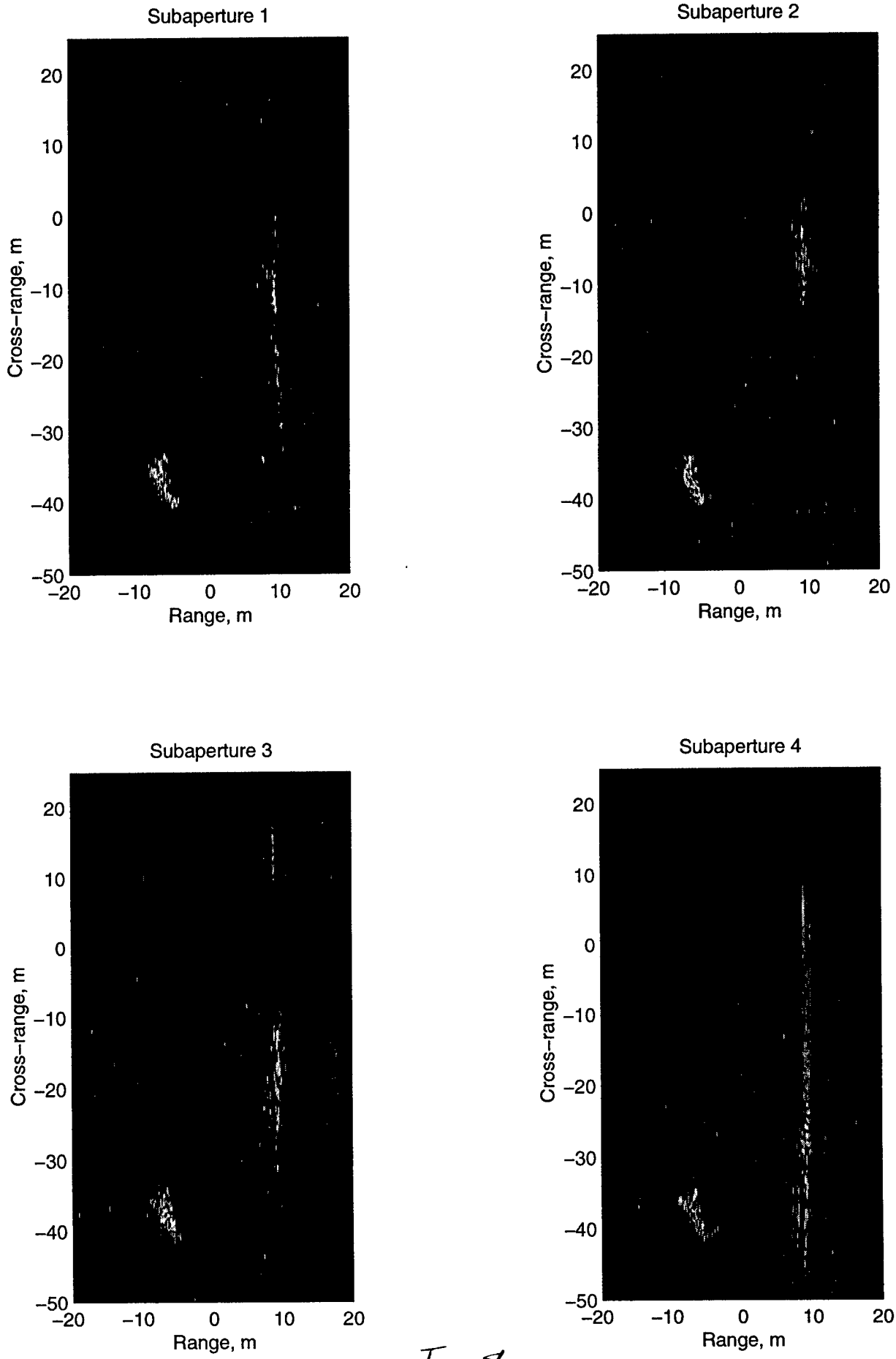
Subaperture 1
Subaperture 2
Subaperture 3
Subaperture 4
Cross–range, m
Range, m
20
10
0
–10
–20
–30
–40
–50
–20
–10
0
10
20

Fig. 8a

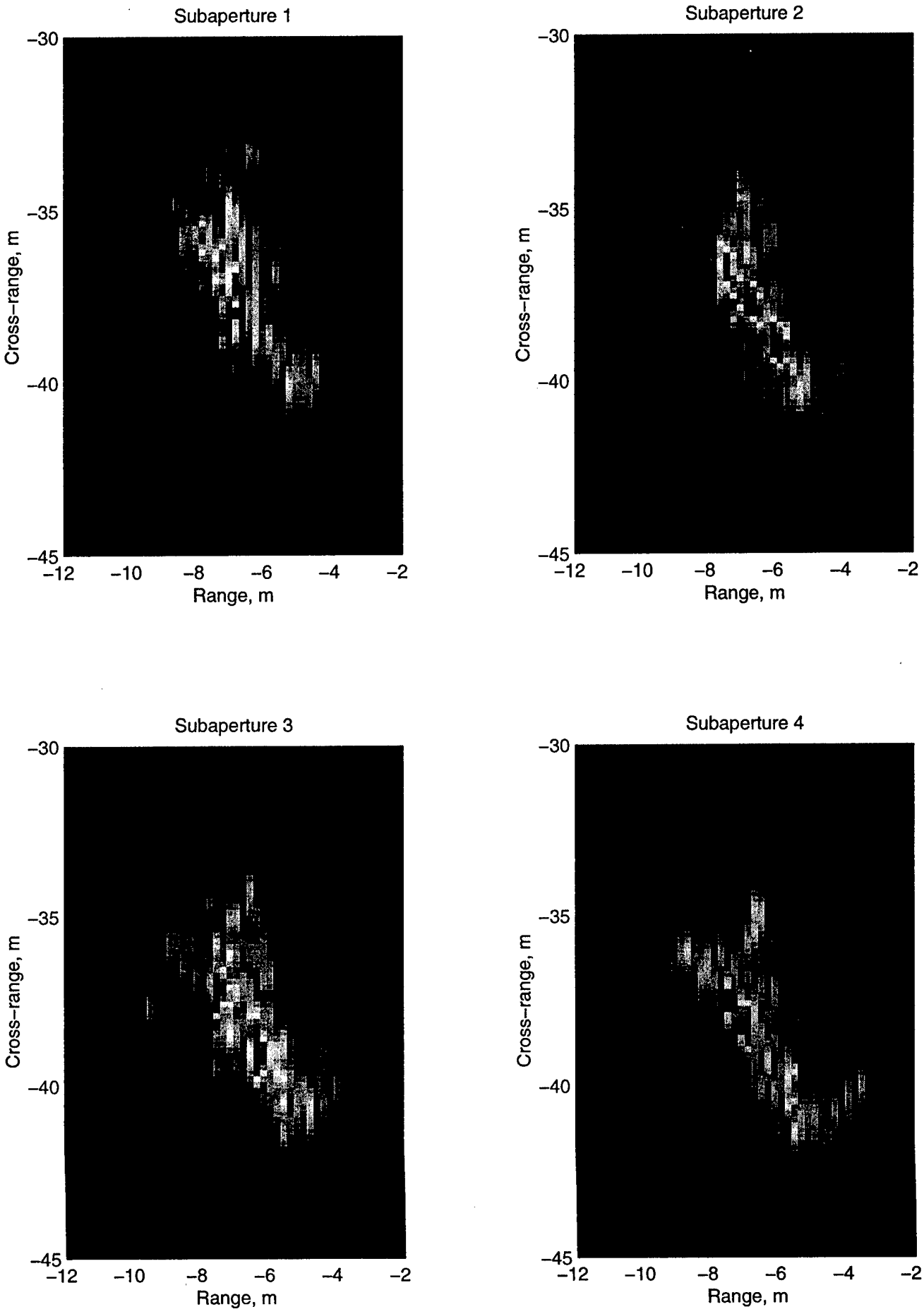
Subaperture 1
Subaperture 2
Subaperture 3
Subaperture 4
Cross–range, m
Range, m
–30
–35
–40
–45
–12
–10
–8
–6
–4
–2

Fig. 8b

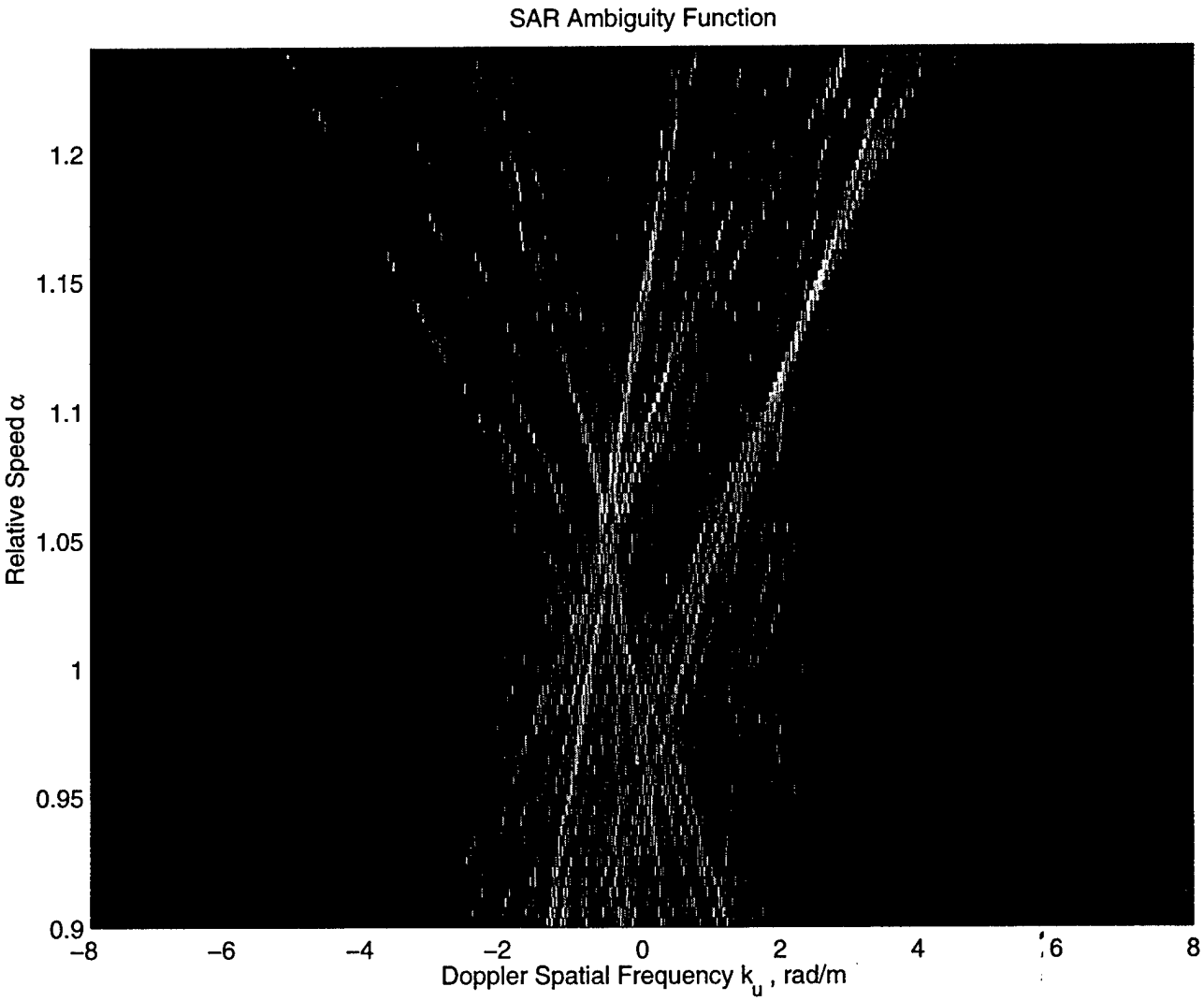
SAR Ambiguity Function
Relative Speed α
1.2
1.15
1.1
1.05
1
0.95
0.9
−8
−6
−4
−2
0
2
4
6
8
Doppler Spatial Frequency k_u , rad/m

Fig. 9

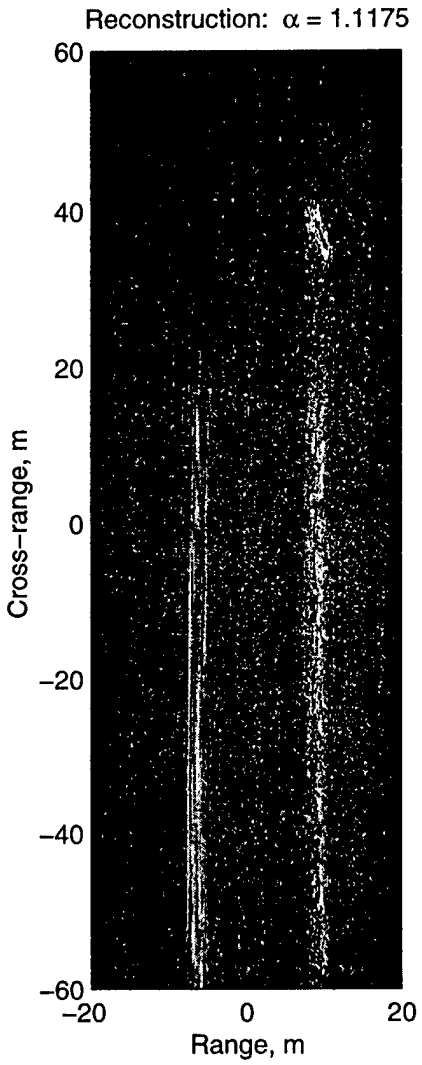
Reconstruction: α = 1.1175
60
40
20
0
−20
−40
−60
Cross−range, m
−20
0
20
Range, m

(a)

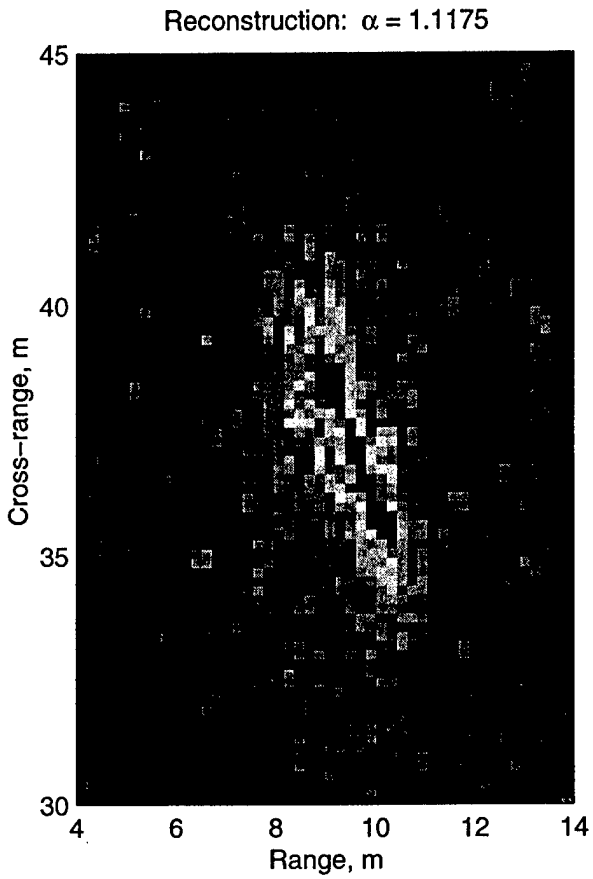
Reconstruction: α = 1.1175
45
40
35
30
Cross−range, m
4
6
8
10
12
14
Range, m

(b)

Fig. 10

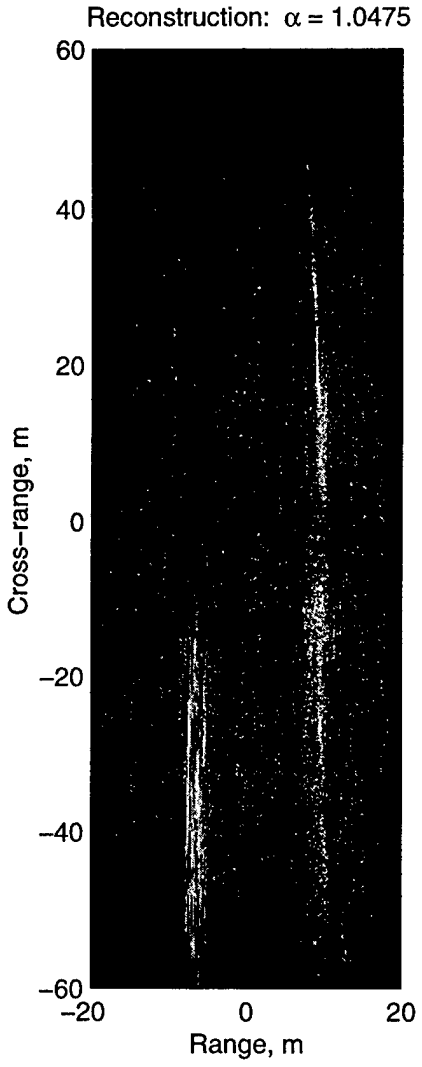
Reconstruction: α = 1.0475
60
40
20
0
−20
−40
−60
−20
0
20
Cross−range, m
Range, m

(a)

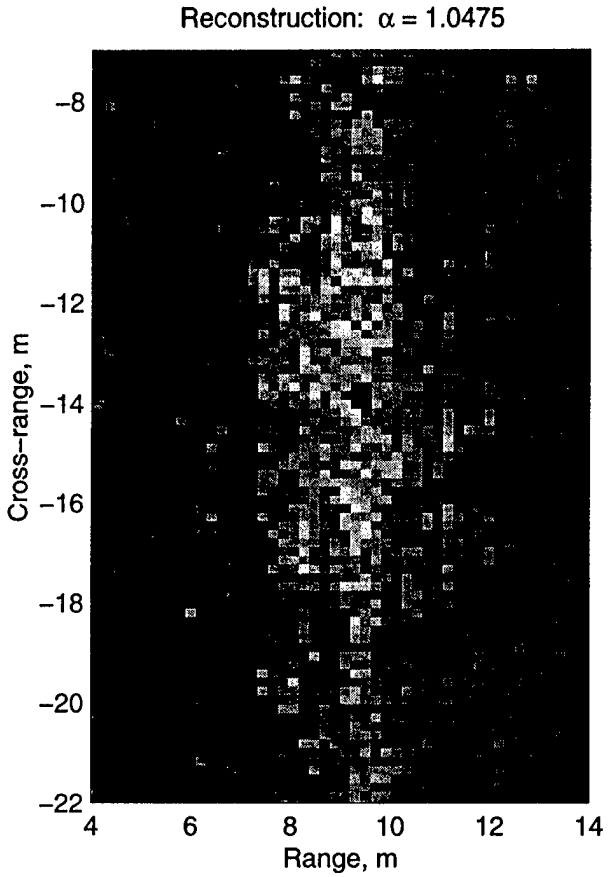
Reconstruction: α = 1.0475
−8
−10
−12
−14
−16
−18
−20
−22
4
6
8
10
12
14
Cross−range, m
Range, m

(b)

Fig. 11

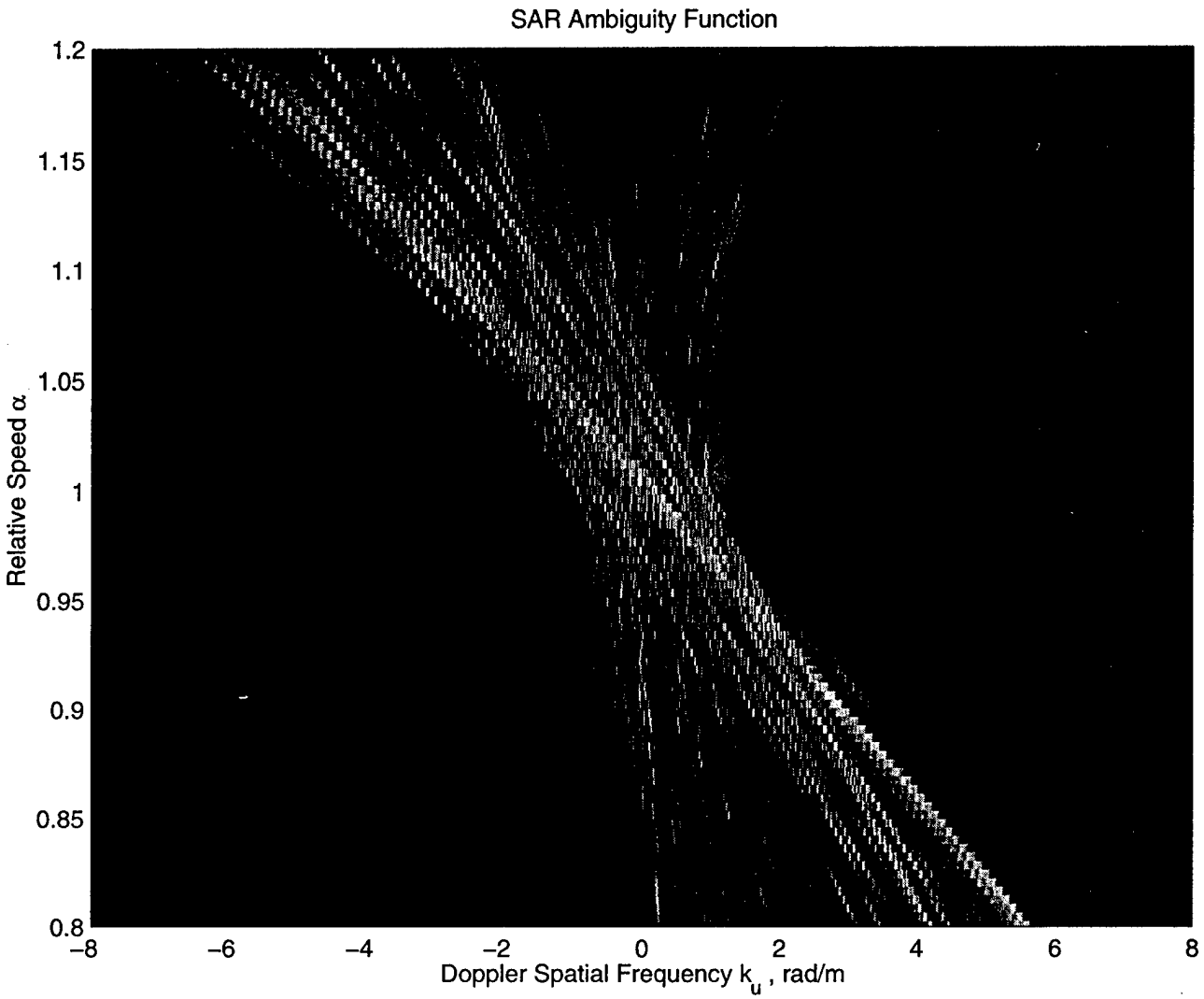
SAR Ambiguity Function
1.2
1.15
1.1
1.05
1
0.95
0.9
0.85
0.8
Relative Speed α
−8
−6
−4
−2
0
2
4
6
8
Doppler Spatial Frequency k_u , rad/m

Fig. 12

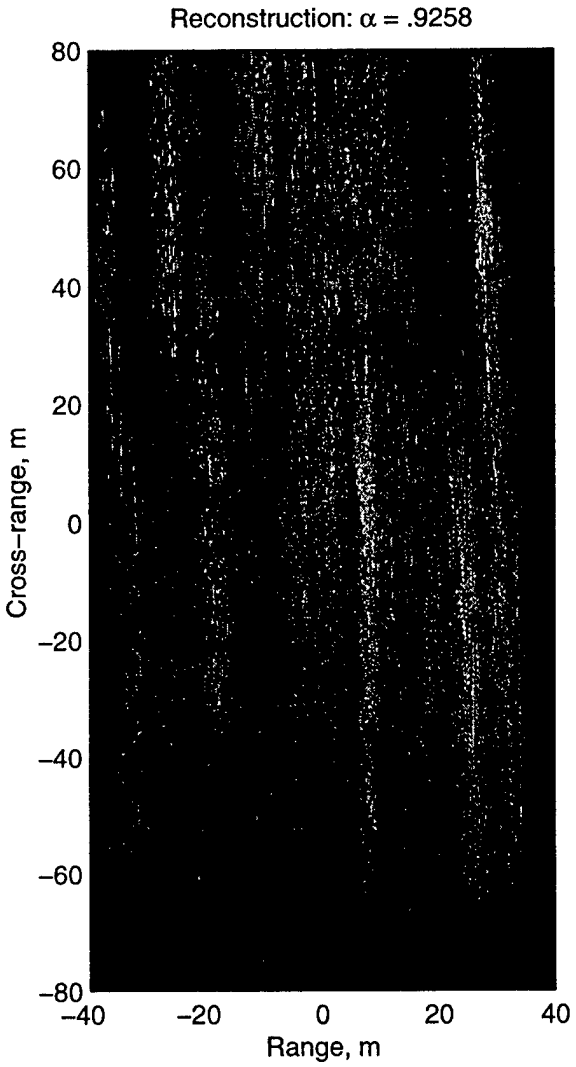
Reconstruction: α = .9258
80
60
40
20
0
−20
−40
−60
−80
Cross−range, m
−40
−20
0
20
40
Range, m

Fig. 13

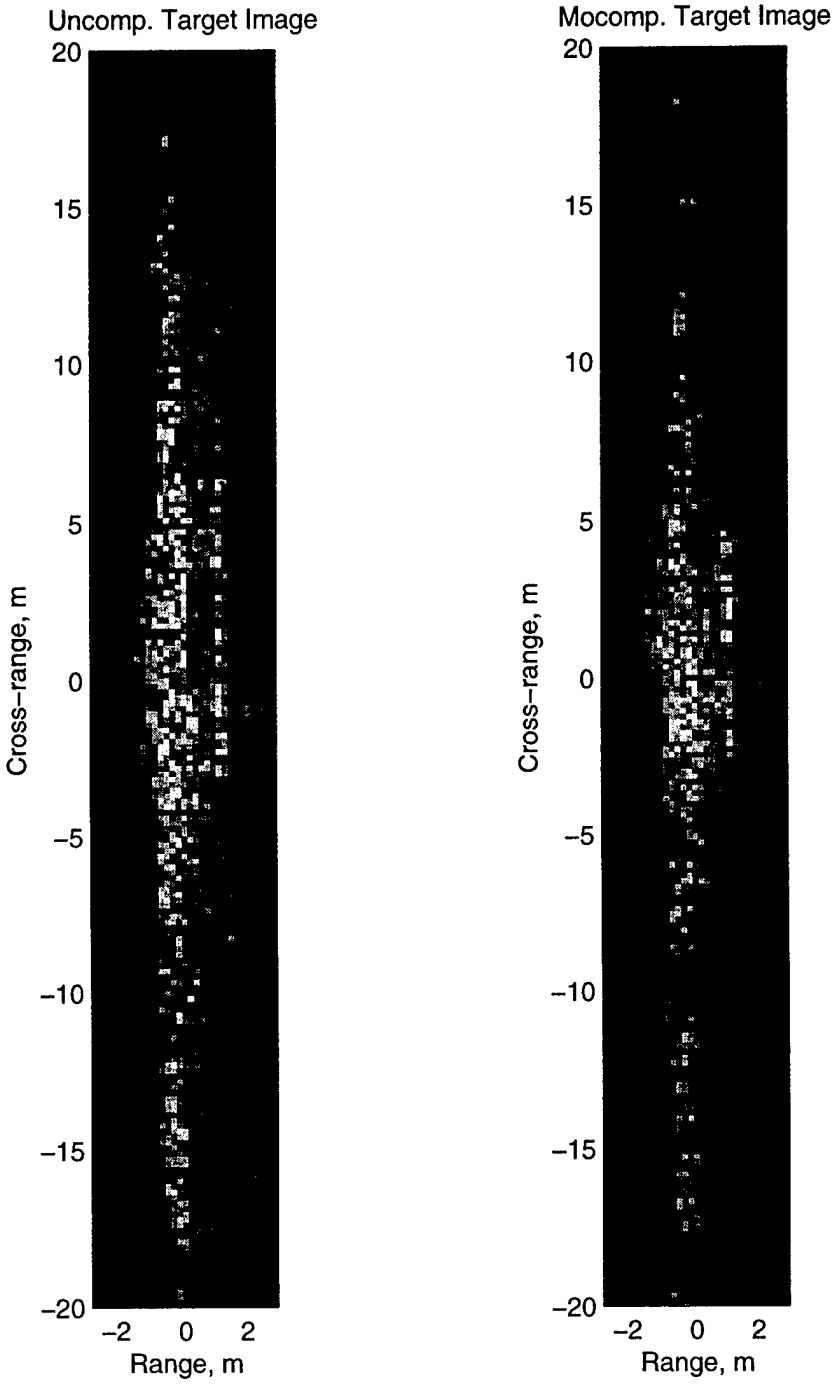
Uncomp. Target Image
Mocomp. Target Image
Cross–range, m
Range, m
20
15
10
5
0
–5
–10
–15
–20
–2
0
2
(a)
(b)

Fig 14

REPORT DOCUMENTATION PAGE

Form Approved
OMB No. 0704-0188

1. AGENCY USE ONLY *(Leave blank)*	2. REPORT DATE	3. REPORT TYPE AND DATES COVERED
	2/20/2002	Final Report

4. TITLE AND SUBTITLE
Signal Subspace Processing of Uncalibrated MTD-SARs

5. FUNDING NUMBERS
N00014-97-1-0966

6. AUTHOR(S)
Mehrdad Soumekh

7. PERFORMING ORGANIZATION NAMES(S) AND ADDRESS(ES)
Department of Electrical Engineering, 332 Bonner Hall
State University of New York at Buffalo
Amherst, NY 14260

8. PERFORMING ORGANIZATION REPORT NUMBER

9. SPONSORING / MONITORING AGENCY NAMES(S) AND ADDRESS(ES)
Office of Naval Research
Ballston Center Tower One
800 North Quincy Street
Arlington, VA 22217-5660

10. SPONSORING / MONITORING AGENCY REPORT NUMBER

11. SUPPLEMENTARY NOTES

a. DISTRIBUTION / AVAILABILITY STATEMENT
Approved for public release

12. DISTRIBUTION CODE

13. This report provides a study on the merits of the algorithms that we have developed under this contract. For this purpose, we present moving target detection and imaging results for an X band spotlight SAR system that utilizes an along-track monopulse configuration for its data collection. The theoretical foundation of the processing that is used on these data is based on our work for this contract in which a two-dimensional signal subspace processing (adaptive filtering) method was developed to calibrate the monostatic and bistatic radars of the monopulse SAR system. The blind calibration of the two channels enables the user to null the stationary scene, and detect the moving targets. Next, a measure that we call SAR ambiguity function is used to estimate the relative speed of a detected moving target. The resultant estimate is then used to image the moving target.

14. SUBJECT TERMS	15. NUMBER OF PAGES
Synthetic aperture radar, moving target detection & imaging	37
	16. PRICE CODE

17. SECURITY CLASSIFICATION OF REPORT	18. SECURITY CLASSIFICATION OF THIS PAGE	19. SECURITY CLASSIFICATION OF ABSTRACT	20. LIMITATION OF ABSTRACT
Uncalssified	Unclassified	Unclassified	